Materials Research Bulletin 145 (2022) 111539

Contents lists available at ScienceDirect

Materials Research Bulletin

journal homepage: www.elsevier.com/locate/matresbu

Research Papers

Photoelectrocatalytic degradation of caffeine using bismuth vanadate modified with reduced graphene oxide

Thiago M. Prado [a], Fernando Lindo Silva [a], Amanda Carrico [a], Marcos Roberto de Vasconcelos Lanza [b], Orlando Fatibello-Filho [a], Fernando C. Moraes [a,*]

[a] Department of Chemistry, Federal University of São Carlos, Rodovia Washington Luis, s/n Km 235, P.O. Box 676, 13560-970 São Carlos, SP, Brazil
[b] São Carlos Institute of Chemistry, University of São Paulo, Avenida Trabalhador São Carlense 400, São Carlos 13566-590, SP, Brazil

ARTICLE INFO

Keywords:
Photoelectrocatalysis
Bismuth vanadate
Reduced graphene oxide
Caffeine
Degradation

ABSTRACT

Bismuth vanadate modified with reduced graphene oxide ($BiVO_4$/rGO) was synthesized with the aim of applying this semiconductor material in advanced oxidative processes (AOPs) using the photoelectrocatalytic properties of the material for caffeine degradation. The semiconductor material was characterized by Scanning electronic microscopy, X-ray diffraction, Raman spectroscopy and UV–Vis Diffuse reflectance spectrophotometry. Photo-assisted linear sweep voltammetry experiments were carried out in order to evaluate the photocurrent generated in the processes. $BiVO_4$/rGO was found to exhibit relatively better photoelectrocatalytic performance compared to bare $BiVO_4$; this result confirms the fundamental role of the carbon-based material when it comes to photoanode construction. With regard to caffeine degradation by high performance liquid chromatography through the application of $BiVO_4$/rGO photoanode, the signal used for monitoring the presence of the analyte exhibited a decrease of 100% of caffeine concentration from the original concentration, indicating the efficient removal of the compound from the sample.

1. Introduction

In recent times, there has been a dramatic rise in indiscriminate discharge of compounds with high contamination potential into the environment. This global phenomenon has led to the appearance of irreversible and hazardous problems, among them including the feminization of some animals and the extinction of their species [1]. Bearing that in mind, many research groups around the world have become increasingly involved in the development of efficient methods in an attempt to address this environmental contamination problem. As part of the efforts to tackle this issue, advanced oxidative processes (AOP) were developed with the aim of removing extra-stable compounds, including synthetic and non-synthetic organic molecules, during the purification of contaminated water from domestic sewage. The fundamental strategy of the AOPs lies in the use of hydroxyl radicals, which are often responsible for the rapid and non-selective oxidation of pollutants. This oxidizing agent is produced through reactions in situ, such as the decomposition of ozone [2], or from combined systems, such as Fenton [3], UV/H_2O_2 [4] or photoelectrochemical generation [5].

The generation of hydroxyl radicals (●OH) through photovoltaic methods is based on the reaction of O_2 production from water photoelectrolysis [6]. In this case, a semiconductor material is used to produce a specific photoanode which acts based on the mechanism known as SMPD (Semiconductor-mediated photodegradation) [7]. The SMPD process is proposed for the operation of the photoanode developed in this work. Several studies published in the literature have reported the use of semiconductor-based photoanodes for the photoelectro-degradation of environmental pollutants [8–12].

Interestingly, one of the most prominent materials for the construction of photoanodes is bismuth vanadate ($BiVO_4$) [13–18]. $BiVO_4$ is an *n*-type semiconductor with interesting properties, including the following: (i) high stability in aqueous medium; (ii) wide range of potential; (iii) adequate position between the valence and conduction bands; (iv) high efficiency in electron transport; and (v) the possession of catalytic activity for O_2 and H_2 release reactions [19]. In particular, compared to other semiconductors, such as TiO_2 [20], which are commonly used in degradation processes, the main advantage of $BiVO_4$ lies in its band gap energy of 2.4 eV when found in monoclinic crystallographic structure [21]. This band gap is suitable for O_2 evolution (1.23 eV), as it promotes water splitting with lower energy consumption

* Corresponding author.
E-mail address: fcmoraes@ufscar.br (F.C. Moraes).

https://doi.org/10.1016/j.materresbull.2021.111539
Received 15 July 2020; Received in revised form 17 August 2021; Accepted 29 August 2021
Available online 1 September 2021

and allows electrons to be excited from the valence band (VB) to the conduction band (CB) under visible light and UV radiation.

Other advantages of $BiVO_4$ that are worth mentioning include the following: the semiconductor requires low electrochemical potential for water splitting, exhibiting high photocurrent values; it does not require the use of strongly acidic or basic media to ensure excellent performance in photoelectrochemical cells (PEC); has low toxicity; and involves less costly synthetic routes [22]. These relevant properties make $BiVO_4$ an interesting material for the degradation of environmental pollutants [23, 24].

Graphene is another promising material that can be employed in photoanodes used in degradation via AOPs. By virtue of its outstanding semiconductor and electrochemical properties, graphene is found to enhance the efficacy of the degradation process. This material has an ambipolar semiconductor characteristic, possessing covalent C–O bonds and plenty of oxygenated functional groups on its surface. Graphene creates a number of charge carriers that can be modulated depending on the degree of oxidation.

Graphene oxide (GO) is a *p*-type semiconductor, which can be converted into *n*-type semiconductor by simply replacing the oxygen groups with nitrogen groups [25], or by the complete transformation of the hybrid orbital sp^3 of GO to sp^2 in reduced graphene oxide (rGO). The large amount of oxygenated groups present in graphene during the synthesis drastically reduces its conductivity. Thus, from an electrochemical viewpoint, rGO presents interesting features; these include large useful window of potential, low resistance to charge transfer, wide surface area and electrocatalytic activity [26]. Clearly, these properties provide the material with great flexibility when it comes to application in photovoltaic systems [27], including those used in AOPs.

Some compounds, such as organochlorines, organophosphates, disinfectants and secondary products of disinfection, are harmful to humans and ecosystems, because of that the use of these compounds and the maximum amount of residues derived from them are regulated and controlled by governmental environmental agencies around the world [28]. However, researchers have discovered other classes of organic molecules, with natural or synthetic origin, including pharmaceuticals and personal care products (PPCPs), which have also been found to produce toxic effects on human health. To date, no specific legislation has yet been promulgated to properly regulate the disposal of these toxic organic molecules in waters, and for that matter, these harmful substances are classified as emerging pollutants [29].

Within this context, caffeine (CAF) is considered an emerging pollutant. CAF is widely used as additive in medicinal drugs because of its cardiac, respiratory and brain stimulating properties. Its presence in surface and groundwater makes it an anthropogenic marker, since it is neither consumed by animals nor it is present in fertilizers [30–32]. When found in aquatic bodies, CAF is often associated with the presence of PPCPs and other organic substances; this allows it to be used as an efficient indicator of environmental pollution [33]. In addition, risk assessment studies have shown that the presence of CAF in aquatic environments produces toxic effects on bacteria and crustaceans [29].

Considering the impact of emerging pollutants found in large scale in nature and the potential application of $BiVO_4$ and rGO in AOPs, the present work reports the synthesis of a nanocomposite material which was, subsequently, used in the construction of photoanodes. The proposed device was employed for caffeine removal from natural water samples in real time.

2. Experimental

2.1. Reagents

The aqueous solutions were prepared with water purified in Milli-Q System, Direct 8 (Millipore, USA), with resistivity $\geq$ 18 MΩ cm. All the reagents used were of analytical grade, and were not subjected to further purification. Ascorbic acid (AA), ammonium tetravanadate, dimethylformamide (DMF), graphene oxide (GO), sodium borohydride, caffeine (CAF) and uric acid (UA) were obtained from Sigma/Aldrich. Isopropanol was obtained from Anidrol/Brazil. Bismuth (III) nitrate pentahydrate and sodium sulfate anhydrous were purchased from Chem-Impex Int'l and Merck, respectively. Sodium sulfate solution (0.1 mol L^{-1}) acidified at pH 3.0 was used as supporting electrolyte. This solution was used as electrolyte in the preparation of 3×10^{-2} mol L^{-1} of CAF standard solutions.

2.2. $BiVO_4$ synthesis

A mass of 0.235 g of ammonium tetravanadate was accurately weighed and placed in a flask containing 10.0 mL of pure water. The mixture was heated in a water bath until complete dissolution of the solids contained therein. Concomitantly, a mass of 0.970 g of bismuth (III) nitrate pentahydrate was accurately weighed and placed in another flask containing 10.0 mL of ethylene glycol; this mixture was sonicated for 40 min. After that, the solution containing vanadate ions was dropped slowly, and with constant stirring, into the bismuth solution, forming a yellowish colored bismuth vanadate ($BiVO_4$) suspension.

2.3. Reduced graphene oxide (rGO) synthesis

Reduced graphene oxide (rGO) was prepared by dispersing 25.0 mg of GO in 25.0 mL purified water via ultrasound for 40 min. Subsequently, the mixture was heated to boiling under continuous magnetic stirring, and then an amount of 12.5 mg of $NaBH_4$ was added to it. The mixture was stirred under heating at 80 °C for another 30 min. Thereafter, the system was cooled to room temperature and filtered. The resulting solid was washed with water and isopropanol, dried under vacuum at room temperature, and kept dry until use. A suspension was prepared with the dispersion of rGO in DMF (1 mg mL^{-1}).

2.4. Preparation of the photoanodes

The deposition of bismuth vanadate ($BiVO_4$) onto FTO glass electrode was performed using a hot plate under the temperature of 100 °C. In the first step, 2.0 mL of fresh $BiVO_4$ suspension were dropped into 20.3 cm^2 of FTO glass electrode. After 2 min, a plastic $BiVO_4$ film was formed. This procedure was repeated twice to guarantee a complete recovery of the FTO surface. Afterwards, the FTO/$BiVO_4$ glass electrode was put in an oven and heated at 500 °C under a heating rate of 10 °C min^{-1}, which was maintained for 1 hour. The heat treatment was needed in order to change the crystalline structure of $BiVO_4$ from the orthorhombic phase to the monoclinic phase, which has the ideal band gap value (2.4 eV) for the application of the material in photoelectrochemical devices [29]. At the end of the process, the modified FTO glass electrode was removed from the oven and allowed to cool in a desiccator. The immobilization of rGO on $BiVO_4$ was performed by dripping the rGO dispersion over the electrode until the surface was covered with a total volume of 1.5 mL. After this step, the electrode was maintained under infrared lamp irradiation to dry.

2.5. Characterization of $BiVO_4$ and $BiVO_4$/rGO films

The morphology of the films was investigated by scanning electron microscopy using JSM-6301F microscope (JEOL, USA). The X-ray diffraction (XRD) analysis was performed with the aid of Bruker D8 Advance diffractometer, using CuK radiation $l = 1.5406$ Å, voltage of 40 kV and theta-2theta configuration, with the sweep angle of 5 – 70 °, and rate of 0006 ° s^{-1}. Raman spectra were obtained using Raman Spectrometer B&W TekModel BWS 415–785H. The hardware was managed by B&WSpec software 4.03–23-C. The following conditions were employed: excitation wavelength of 785 nm, integration time of 60 s, and laser power varying from 31.6 to 316.0 mW. In order to estimate the optical band gap of the materials, UV–vis spectra were obtained using

Varian Cary 5 G UV–vis-NIR spectrophotometer in the diffuse reflectance mode.

2.6. Photoelectrochemical and degradation experiments

Photocurrent measurements were performed using PGSTAT-204 Autolab electrochemical system (Eco Chemie, Utrecht, Netherlands), coupled to a LED driver kit Autolab (Eco Chemie, Utrecht, Netherlands), with UV-C led used as irradiation source. The photoelectro-degradation reactor consisted of a special electrochemical cell as shown in Fig. 1S (supplementary material). The quartz window and the four electrodes used were: 2 FTO glass electrode modified with $BiVO_4$/rGO (20.3 cm^2) used as working electrode (photoanode); Ag/AgCl (3.0 mol L^{-1} KCl) employed as reference electrode; and a platinum foil used as counter electrode (20.3 cm^2). To conduct the photo-assisted degradation experiments, the system was irradiated by a UV-C lamp placed into a quartz tube located in the cell center. The chronoamperometry technique was used at a fixed potential of +2.0 V for 8 h. Two degradation studies were also carried out, using the same parameters described above, modifying only the degradation system: degradation using light (photodegradation) only and degradation using current (electrodegradation) only. Measurements were performed in triplicates at 25 °C.

2.7. Analytical procedures

To conduct the study on degradation kinetics, aliquoting was performed during the time studied, and the decrease of caffeine concentration was initially followed by spectrophotometry in the UV–Vis region and high-performance liquid chromatography (HPLC). Shimadzu model UV-1280 UV–Vis spectrophotometer was used to carry out the UV measurements. Spectra were obtained using a 1.0 cm quartz cuvette of optical path ranging from 200 to 600 nm. HPLC experiments were performed using Prominence Shimadzu LC-20AT chromatograph, consisting of a modular system with two CBM-20A pumps, a CTO-10AS oven, a SIL-20A automatic sampler, a SPD-20A variable wavelength detector, and LC-10 workstation class data processor (Shimadzu, Japan). Phenomenex Luna C-18 (5μ) column protected by Supelcosil C-18 protective pre-column was employed. The mobile phase consisted of a mixture of 50% methanol and 50% water (acidified with formic acid). The chromatographic conditions were: 35 °C oven temperature, flow rate of 0.8 mL min^{-1}, UV detection at 280 nm, retention time of 5.2 min and analysis time of 10 min.

3. Results and discussion

3.1. Morphological and structural characterizations

The morphology of the materials employed in the construction of the photoanodes prepared with $BiVO_4$ and $BiVO_4$/rGO films was evaluated using scanning electron microscopy (FEG-SEM), as shown in Fig. 1. The $BiVO_4$ on the FTO surface has characteristic structure of monoclinic crystalline phase, being porous, with wormlike morphology [34] (see Fig. 1A).

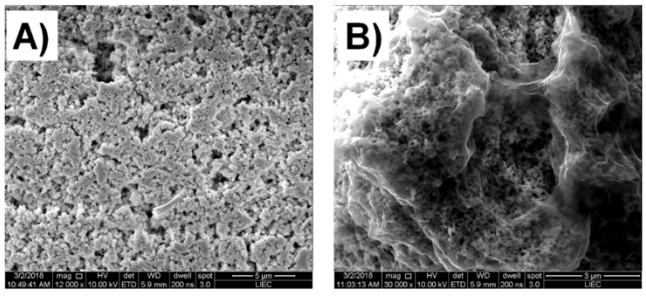

Fig. 1. FEG-SEM micrographs of the photoanodes: (A) FTO/$BiVO_4$ and (B) FTO/$BiVO_4$/rGO.

Fig. 1B shows the surface modification of $BiVO_4$ with rGO. As can be observed, the $BiVO_4$ film is covered by rGO foils evidenced by the edge regions delimited by light contrast. The rGO is transparent enough to allow the observation of $BiVO_4$ located at the bottom of the foils. The degree of transparency is essentially important for the penetration of UV-C radiation through the material structure, providing radiant energy for all regions of the nanocomposite.

Structural characterizations of $BiVO_4$ and $BiVO_4$/rGO films were performed using X-ray diffraction spectroscopy (XRD) (see Fig. 2). The XRD pattern for $BiVO_4$ shows distinct crystallite peaks at 18.8°, 28.8°, 30.5° and 34.6°, which represent the crystalline phases (011), (112), (004) and (020), respectively. These phases are in agreement with the diffraction standard for a monoclinic phase of $BiVO_4$ [35]. Furthermore the use of the Scherrer's equation allowed the calculation of the average crystallite size of $BiVO_2$, resulting in the value of 32 nm.

The XRD pattern for rGO presents a large and low intensity peak at 24.1°; this corresponds to an interlayer spacing of 3.708 Å according to Bragg's law: $2d\sin\theta = n\lambda$ ($\lambda = 1.54$ Å). These observations are related to the chemical reduction of oxygenated functional groups of the precursor, GO, and the decrease of initial interlayer spacing with typical value of 7.599 Å, as reported in the literature [36]. A comparison between the XRD patterns of the isolated materials ($BiVO_4$ and rGO) and the nanocomposite ($BiVO_4$/rGO) showed that the hybrid material has been synthesized as expected due to the presence of narrow peaks belonging to $BiVO_4$ at 18.8° and 30.5° and the typical rGO peak at 24.1°.

Raman spectra experiments were performed for the analysis of the local structure and bonding states of the nanocomposite. These experiments were conducted in order to confirm the presence of $BiVO_4$ and rGO in the hybrid material. Fig. 3 shows the Raman spectra for $BiVO_4$ and $BiVO_4$/rGO. In the $BiVO_4$ spectrum, the narrow and intense band observed at 825 nm is attributed to the stretching modes of V–O bonds; this indicates the contribution of Bi^{3+} ions for the distortion of the unit cell structure of $BiVO_4$ [35]. The stretching modes can be affected by factors, such as doping, crystallite facet, morphology variation and defects creations. In addition, the bands from 150 nm to 360 nm correspond to the symmetric deformation modes of VO_4^{3-} tetrahedron [35].

The $BiVO_4$/rGO spectra presented the characteristic bands of $BiVO_4$ and the typical bands of rGO. The typical rGO bands can be observed in detail in Fig. 3. The characteristic *D* and *G* bands observed in the spectrum confirm the presence of rGO in the nanomaterial structure [32]. Another relevant information that confirms the presence of rGO is the relative intensity of the bands, presenting an I_D/I_G value of 1.62; this is related to the different types of lattice defects which are expected for rGO [37]. These defects have direct influence on the electronic mobility

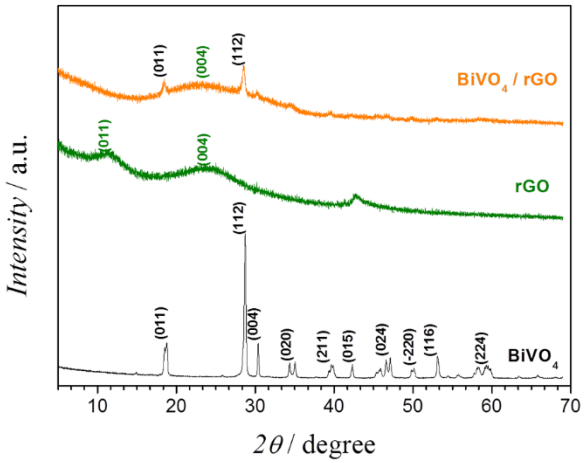

Fig. 2. XRD patterns for the materials: $BiVO_4$, rGO and $BiVO_4$/rGO.

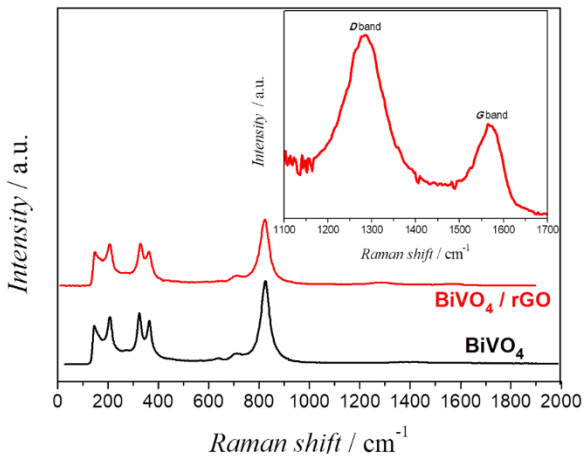

Fig. 3. Raman Spectra for $BiVO_4$ and $BiVO_4$/rGO.

in the rGO structure, due to the formation of ribbons that act as quantum dots or waveguides, allowing the electrons to flow freely [37].

3.2. Photoelectrochemical and spectrophotochemical characterizations

The photoelectrochemical behavior of $BiVO_4$ and $BiVO_4$/rGO photoanodes was evaluated using linear scanning voltammetry (LSV) at potential range of 0.0 V to +2.0 V, with scan rate of 25 mV s^{-1}, in an electrochemical cell with quartz window under on/off irradiation system coupled to a UV-C led lamp. By analyzing the LSV voltammograms shown in Fig. 4, both materials can be found exhibiting photocurrent responses at the potential range scanned. As expected, $BiVO_4$ presented a photocurrent signal related to the interaction between the monoclinic crystalline phase of the semiconductor and the incident radiation. However, the photocurrent of the nanocomposite, $BiVO_4$/rGO, was found to be higher than that of $BiVO_4$ in all the potential range scanned. These results are attributed to the presence of rGO, which acts by photosensitizing $BiVO_4$ and increasing the photocurrents responses at about 56% higher than those of bare $BiVO_4$. The maximum photocurrents responses observed at the potential range of + 1.0 V to + 2.0 V are attributed to the water splitting reaction prompted by the semiconductor under illumination. When the semiconductor was irradiated at the potential between + 1.0 V and + 2.0 V, the electrons belonging to the semiconductor material were promoted from the VB to CB, and holes were produced on the semiconductor surface. Based on the reaction

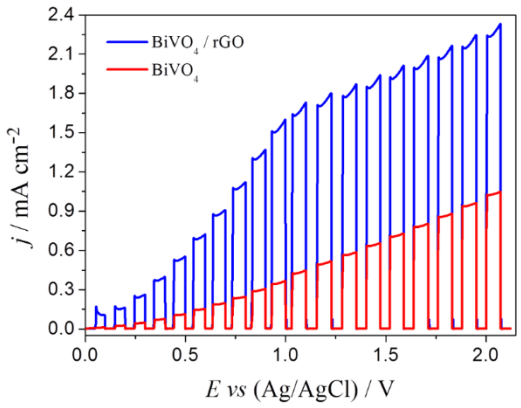

Fig. 4. Linear scanning voltammograns of the $BiVO_4$/rGO (blue line) and $BiVO_4$ (red line) electrodes, obtained in 0.1 mol L^{-1} Na_2SO_4 solution (pH = 3.0), scan rate 25 mV s^{-1}, under on/off irradiation with a hot white LED (λ > 410 nm). (For interpretation of the references to colour in this figure legend, the reader is referred to the web version of this article.)

represented in Eq. (1), the water splitting phenomenon is caused by the holes (h_{vb}^+), leading to the generation of hydroxyl radical and a hydrogen proton.

$$H_2O + h_{vb}^+ \rightarrow \bullet OH + H^+ \quad (1)$$

This is an interesting feature of the proposed photoanode in the sense that the hydroxyl radical generated acts on the target molecule aiming at its degradation. Considering the higher potential applied (+2.0 V), higher degradation efficiency was expected.

In addition, the photosensitizer effect of rGO was demonstrated through optical band gap estimation, using the diffuse reflectance spectroscopy (DRS) and the Kubelka-Munk function to determine the absorption coefficient of $BiVO_4$/ rGO [38]. The calculations were made from spectra presented in Fig. 5B and Fig. 5C. Fig. 5A shows the resultant Tauc plot, where the band gap of the nanocomposite material was calculated by the extrapolation of the linear range to the abscissa axis [38]. The E_g value obtained was 2.02 eV for the $BiVO_4$/rGO, whereas for the $BiVO_4$ was 2.04 eV; these are less than the characteristic band gap of $BiVO_4$ (2.40 eV) due the formation of crystalline nanoparticles [39]. The decrease in band gap stemming from the presence of rGO is attributed to the overlapping of the bands related to rGO with those of $BiVO_4$.

In addition, data from electrochemistry impedance spectroscopy experiments are summarized in the Table 1 and Fig. 6, which demonstrated the decrease of the resistance of charge transfer in caffeine oxidization due the rGO presence, corroborating that the efficiency of the photoanode might be increased with the carbonaceous material. These experiments were performed for FTO, FTO/$BiVO_4$ and FTO/$BiVO_4$/rGO in the presence of 10 μmol L^{-1} of caffeine, at +2.0 V in 0.1 mol L^{-1} Na_2SO_4 (acidified, pH = 3.0). Nyquist plots data were fitted using an equivalent electrical circuit with a cell resistance, R_Ω, in series with the parallel combination of a charge transfer resistance, R_{ct}, and a constant phase element, *CPE*. The rGO contributes for the efficiency of the caffeine electro-oxidization, with decreasing of the resistance in the charge transfer under the photoanode irradiation (from 3.17 kΩ to 1.21 kΩ). This behavior can be explained based on the presence of functional groups onto rGO foils that causing the bypassing of the electrons from the electro-oxidation process to the VB, where they are collected by the holes. The rGO 2D structure has sp2 carbons and so the charge transfer from the electrode surface to the VB of $BiVO_4$ is very fast and contributes to the increase of the electro-oxidization process efficiency [40].

3.3. Degradation of caffeine using FTO/$BiVO_4$/rGO photoanode

The degradation of caffeine was investigated using a photoelectrochemical reactor and chronoamperometry technique at fixed potential of +2.0 V for 8 h with 0.1 mol L^{-1} solution of Na_2SO_4 (pH = 3.0) containing 10 μmol L^{-1} of caffeine.

The electrolysis inspection was performed using spectrophotometry in the region of UV–Vis (200–600 nm). At specific time intervals, aliquots of the sample were collected and analyzed in the UV–Vis spectrum in order to evaluate the kinetic decay curve of caffeine concentration.

For comparison purposes, four types of caffeine degradation procedures were employed: (A) photodegradation (in the absence of applied potential); (B) electro-degradation using FTO/ $BiVO_4$/rGO as anode (in the absence of light); (C) photoelectron degradation using FTO/$BiVO_4$ photoanode; (D) photoelectron degradation using FTO/$BiVO_4$/rGO photoanode. The spectra are shown in Fig. 7.

The characteristic spectrum of caffeine has an absorption in the region between 245 and 295 nm. The maximum intensity of this absorption depends greatly on the solvent used. The band with maximum absorbance at 276 nm is related to the chromophore center $C = O$ present in caffeine molecule [41]. By analyzing Fig. 7A, it observes that the sole application of ultraviolet light irradiation (UV-C) on the sample of caffeine contributes to a decrease in caffeine concentration. Similarly, looking at Fig. 7B, one notices that the use of FTO/$BiVO_4$/rGO

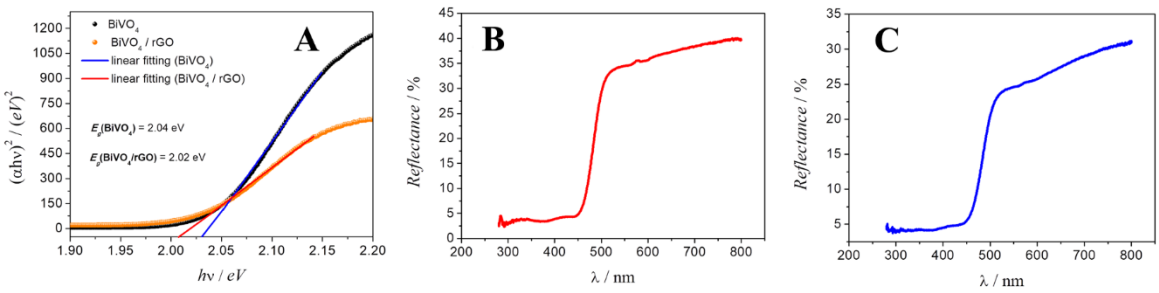

Fig. 5. (A) Tauc plots of the $BiVO_4$ and $BiVO_4$/rGO with Kubelka-Munk function applied to diffuse reflectance spectra. (B) $BiVO_4$ and (C) $BiVO_4$/rGO spectra obtained from UV–Vis spectrophotometry.

Table 1
Parameters of the electrical equivalent circuits.

Electrode	R_s / Ω	R_{ct} / Ω	[C] / μF
FTO (off)	−117.8	385,300	4.13
FTO (on)	−156.9	561,650	2.83
$BiVO_4$ (off)	−738.5	264,470	6.02
$BiVO_4$ (on)	53.2	4083	0.27
$BiVO_4$/rGO (off)	39.5	3168	0.14
$BiVO_4$/rGO (on)	54	1213	0.13

photoanode alone at potential of +2.0 V, in the absence of electromagnetic radiation, leads to caffeine degradation. In these two initial experiments, although caffeine molecule was found to undergo degradation, the reduction percentage was insignificant.

Remarkably, the best degradation results were obtained by the photo-assisted electrochemical technique. Fig. 7C shows caffeine degradation spectra obtained via the application of FTO/$BiVO_4$ electrode in the presence of light. By analyzing the spectra, it observes that a significant portion of the caffeine was degraded after 8 h of photoelectrolysis. This can be confirmed by the decay of the maximum absorption band at 275 nm in addition to the formation of a by-product detected at the wavelength of 375 nm. Looking at Fig. 6D, when the photoelectrodegradation technique using FTO/$BiVO_4$/rGO was employed, it notices that, although all the caffeine concentration was degraded after 6 h of treatment. The absence of "shoulder" in absorbance spectra suggest that none by-product could be identified using spectrophotometric method. Complementary experiments are must to confirm the existence of by-products, but this is not the purpose of present work.

Additionally, through these results is inferred that the presence of rGO avoids the electron/hole recombination in semiconductor of photoanode and contributes to the increase of hydroxyl radicals generation, which are high reactive and could promote the fully caffeine degradation. All these observations can be better visualized on the decay curve related to the relative concentration of caffeine versus time; this is shown in Fig. 8.

Considering the maximum absorbance of caffeine in the UV–Vis spectra (275 nm), curves of normalized concentrations versus time were constructed. The curves were plotted based on the normalized concentration of caffeine versus degradation time, as shown in Fig. 8. As can be observed, the degradation technique based solely on UV light (curve D) exhibited a decrease of 23.3% in caffeine concentration. The chronoamperometry degradation technique involved the application of + 2.0 V potential and the absence of light (curve C), presented caffeine degradation rate of 25.8%. The experiments presented in curves A and B exhibited much greater degradation efficiency compared to those depicted in curves C and D. The increase observed in degradation efficiency is attributed to the synergic effect that occurred between the chemical oxidation of caffeine (because of the presence of hydroxyl groups produced from light interaction and the $BiVO_4$ semiconductor) and the application of a potential for the electro-oxidation of caffeine. In curve A, a degradation rate of 74.9% is observed; however, as aforementioned, the presence of reduced graphene oxide in the photoanode material significantly improved the material properties, prompting 100% caffeine degradation after 6 h of photo-electrolysis (curve B).

Caffeine degradation process mediated by hydroxyl radicals has been a subject of investigation among several researchers. Using reactive diamonds, Indermuhle et al. [42] performed and monitored the degradation of caffeine by detecting intermediates through electrochemical oxidation. According to these authors, the intermediate products formed stemmed from the opening of the pyrimidine ring after the breakage of part of the imidazole. Dalmazio et al. [43] studied caffeine degradation by-products using three distinct degradation processes based on AOPs: UV/H_2O_2, TiO_2/UV and Fenton system. Interestingly, the three distinct techniques applied yielded the same products, namely, parabamic acid and its 1,3-dimethyl derivative. In another related study, Telo and Vieira [44] showed that one of the by-products of caffeine degradation mediated by photocatalytically generated hydroxyl and persulfate radicals is trimethyluric acid. The same authors have also reported to have identified other intermediates by GC–MS; the intermediates included 1,

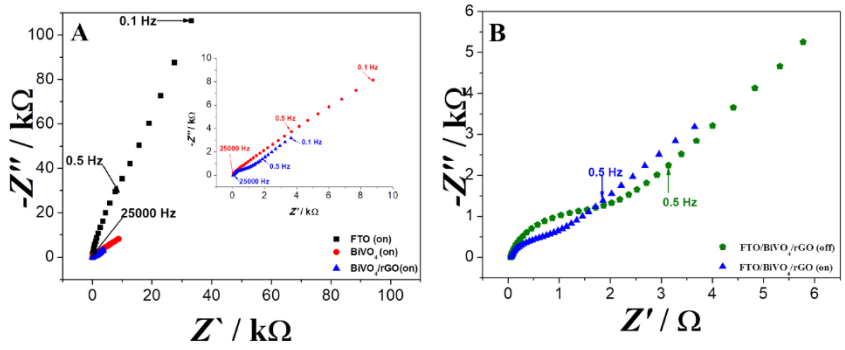

Fig. 6. Nyquist plots: (A) under UV-C irradiation for the comparison between different work electrodes. Inset: detailed plots of the modified FTO glass electrode with BiVO4 (●) and BiVO4/rGO (▲); (B) on/off plots of the $BiVO_4$/rGO. All measures were performed in the frequency range from 25 kHz to 1 mHz.

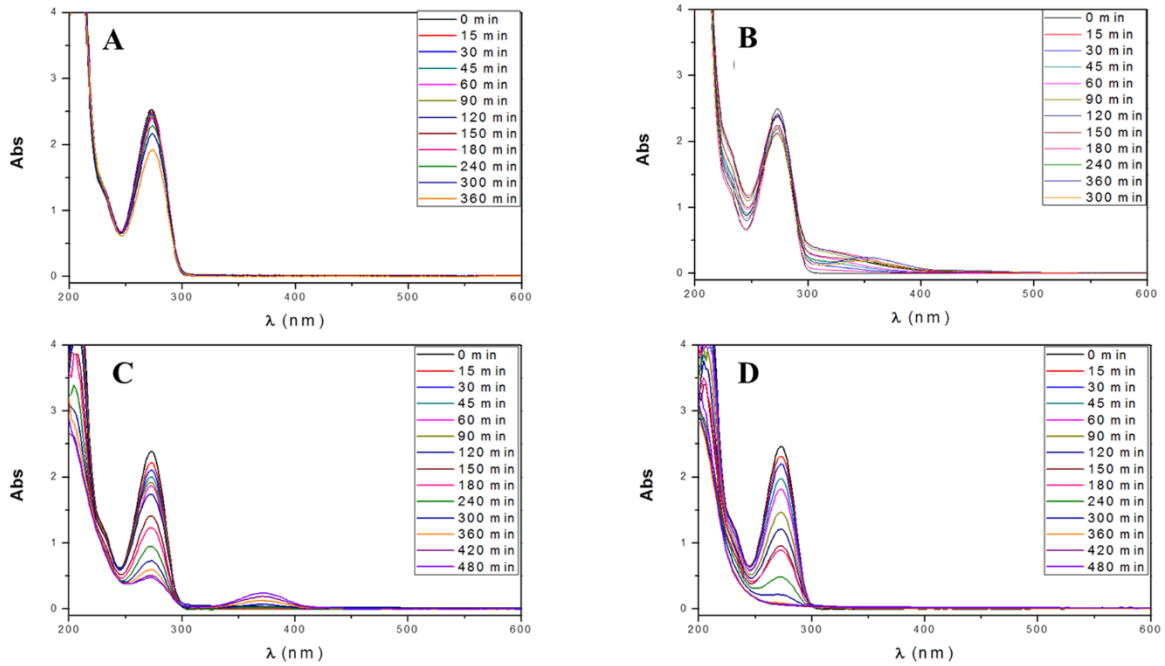

Fig. 7. UV–Vis spectra of the caffeine degradation: (A) photodegradation (in the absence of potential application); (B) electrodegradation using FTO/$BiVO_4$/rGO as anode (in the absence of light); (C) photoelectron-degradation using FTO/$BiVO_4$ photoanode; (D) photoelectrodegradation using FTO/$BiVO_4$/rGO photoanode.

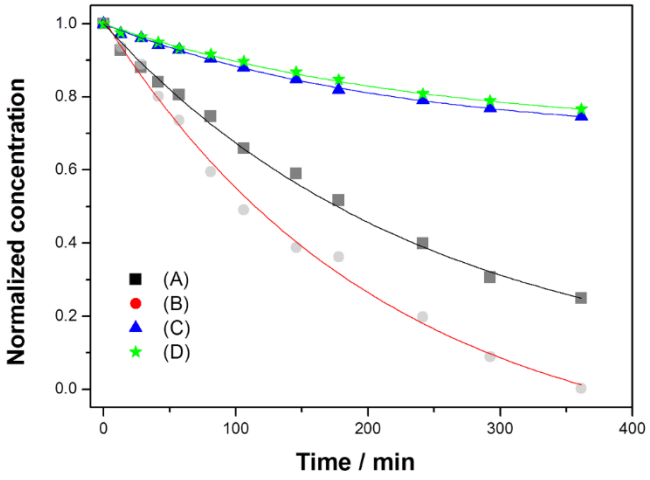

Fig. 8. Decay curve of caffeine relative concentrations versus time, during 6 h under the following conditions: (A) photoelectrodegradation using FTO/$BiVO_4$ photoanode; (B) photoelectrodegradation using FTO/$BiVO_4$/rGO photoanode; (C) electrodegradation using FTO/$BiVO_4$/rGO as anode (in the absence of light) and (D) photodegradation (in the absence of potential application).

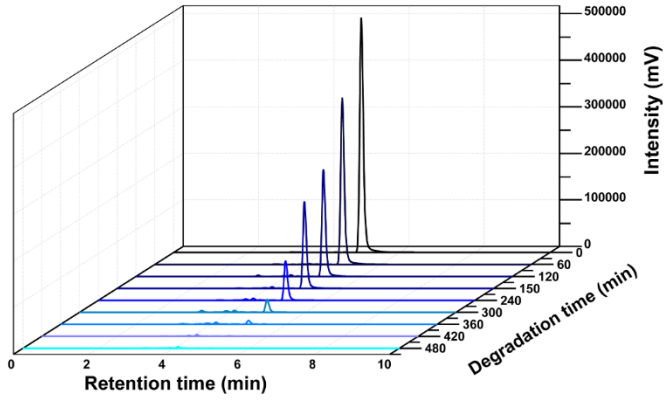

Fig. 9. Chromatograms with retention time at 5.2 s for representative samples of caffeine degradation in a period of 8 hour.

3-dimethylparabane acid and some aliphatic compounds, such as acetic acid, glycerol, acetamide and urea. These generated aliphatic molecules can be mineralized to carbon dioxide and inorganic ions.

In order to obtain better accurate results, monitoring of the photo-electro-oxidation process of caffeine was performed by HPLC measurements. Aliquots from the caffeine degradation process were collected during 8 h, and caffeine degradation was monitored at retention time of 5.2 min. Fig. 9 shows the chromatograms for caffeine in an 8 hour photoelectrodegradation experiment using FTO/$BiVO_4$/rGO photoanode. As can be noted, after the 6 h experiment period, the chromatographic peak related to caffeine was still visible, yet at much lower concentration; the caffeine was not totally eliminated. Through the application of the same experiment technique for 7 h, the characteristic peak of caffeine was found to be no longer detectable, and caffeine was found to have been completely eliminated in the degradation process.

Fig. 10A shows the decrease of relative caffeine concentration versus degradation time for the two distinct processes using $BiVO_4$ (■) and $BiVO_4$/rGO (●). The linearization of these data (see Fig. 10B) in the time range of 0 to 240 min allowed the determination of the apparent velocity constant (k) through the slope of the straight line for both experiments. Considering that the degradation occurred as pseudo-first order reaction, the calculated k values for $BiVO_4$ and $BiVO_4$/rGO were $4 \times 10^{-3}\, s^{-1}$ and $7 \times 10^{-3}\, s^{-1}$, respectively. As expected, the highest k value obtained for $BiVO_4$/rGO confirmed that $BiVO_4$/rGO presented better photoelectrocatalytic efficiency compared to bare $BiVO_4$. After 6 h of experiment, the FTO/$BiVO_4$ photoanode reached 81.7% caffeine removal rate; the removal rate rises to 94.2% after 8 h of treatment. Unsurprisingly, the use of FTO/$BiVO_4$/rGO electrode led to 100% removal rate of caffeine after 6 h of treatment; this result indicates that the use of the composite semiconductor material along with the photoanodes developed in this work can be a promising alternative for the remediation of emerging pollutants in the environment.

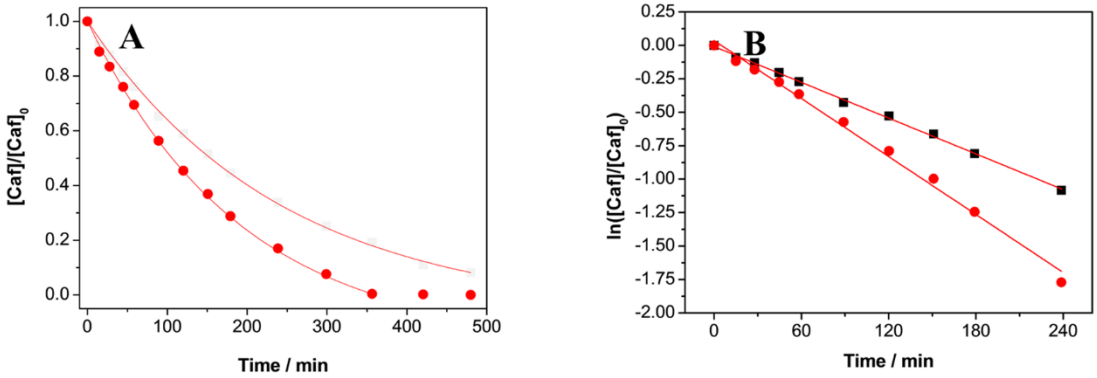

Fig. 10. (A) Decay curves of caffeine relative concentrations during the degradation in a period of 8 h. (B) Linearized data for k values determination. Representation: photoelectrodegradation using FTO/$BiVO_4$ photoanode and (■) photoelectrodegradation using FTO/$BiVO_4$/rGO photoanode (●).

4. Conclusions

A semiconductor material was used for the development of a photoelectrochemical device, which was applied toward the removal of caffeine from samples containing environmental pollutants. The properties of the semiconductor material were used to promote the photocatalysis of water oxidation associated with water splitting under controlled potential of + 2.0 V. Morphological, structural and electrochemical characterization analyses showed that the use of synthesized composite material $BiVO_4$/rGO along with the photoanodes constructed from the composite films deposited on FTO resulted in excellent photocurrent response. The composite material presented suitable band gap energy for photoelectrocatalysis, $E_g = 2.02$ eV, as confirmed by DRS experiments. The FTO/$BiVO_4$/rGO technique involves the oxidation of caffeine through the synergy of chemical and electrochemical (CE) mechanisms, in which the oxidation process is based on photoelectrodegradation mechanism mediated by a semiconductor and initiated by the injection of electrons on the surface of the material. The electronic properties of the proposed hybrid material present great efficiency when it comes to electro-oxidation of environmental pollutants. The material proposed in this work was employed in caffeine degradation, where it produced excellent rates of caffeine removal.

CRediT authorship contribution statement

Thiago M. Prado: Conceptualization, Methodology, Data curation, Writing – original draft. **Fernando Lindo Silva:** Investigation, Writing – review & editing. **Amanda Carrico:** Investigation, Data curation. **Marcos Roberto de Vasconcelos Lanza:** Resources, Writing – review & editing, Funding acquisition. **Orlando Fatibello-Filho:** Resources, Writing – review & editing, Visualization, Funding acquisition. **Fernando C. Moraes:** Resources, Writing – review & editing, Visualization, Supervision, Project administration, Funding acquisition.

Declaration of Competing Interest

None.

Acknowledgements

The authors are grateful the financial support provided by the Brazilian research funding agencies, including the Brazilian National Council for Scientific and Technological Development - CNPq (grants 302874/2017–8, 427452/2018–0 and 405546/2018–1), São Paulo Research Foundation (FAPESP – grants 2014/50945–4, 2017/10118–0 and 2020/01050–5), and the Coordination for the Improvement of Higher Education Personnel (CAPES – Finance Code 001).

Supplementary materials

Supplementary material associated with this article can be found, in the online version, at doi:10.1016/j.materresbull.2021.111539.

References

[1] J. Lintelmann, A. Katayama, N. Kurihara, L. Shore, A. Wenzel, Pure Appl. Chem. (2003) 631.
[2] R. Broséus, S. Vincent, K. Aboulfadl, A. Daneshvar, S. Sauvé, B. Barbeau, M. Prévost, Water Res. 43 (2009) 4707–4717.
[3] X. Liu, C. Wang, M. Ji, Y. Zhou, Environ. Prog. Sustainable Energy 35 (2016) 772–778.
[4] S. Miralles-Cuevas, I. Oller, J.A.S. Pérez, S. Malato, Water Res. 64 (2014) 23–31.
[5] D. Zigah, J. Rodriguez-Lopez, A.J. Bard, Phys. Chem. Chem. Phys. 14 (2012) 12764–12772.
[6] A. Fujishima, K. Honda, Nature 238 (1972) 37.
[7] C. Chen, W. Ma, J. Zhao, Chem. Soc. Rev. 39 (2010) 4206–4219.
[8] S.J. Chang, Q.B. Wang, B.S. Liu, Y.H. Sang, H. Liu, Cataly. Sci. Technol. 7 (2017) 524–532.
[9] R.M. Fernandez-Domene, R. Sanchez-Tovar, B. Lucas-Granados, M.J. Munoz-Portero, R. Ramirez-Grau, J. Garcia-Anton, J. Environ. Manage. 226 (2018) 249–255.
[10] S. Wahyuningsih, C. Purnawan, P.A. Kartikasari, N. Praistia, Chem. Pap. 68 (2014) 1248–1256.
[11] S. Wahyuningsih, A.H. Ramelan, R. Hidayat, G. Fadillah, H. Munawaroh, L. Saputri, Q.A. Hanif, Alternative natural dyes in water purification: anthocyanin as TiO2-sensitizer in rhodamine B photoelectrodegradation, in: T. Omatsu, Y. Hayasaki, Y. Ogura, Y. Ozeki, S. Ohno (Eds.) Biophotonics Japan 2015, 2015.
[12] Q.X. Zhou, A. Xing, D.C. Zhao, K.F. Zhao, Chemosphere 165 (2016) 268–276.
[13] S.K. Pilli, T.G. Deutsch, T.E. Furtak, L.D. Brown, J.A. Turner, A.M. Herring, Phys. Chem. Chem. Phys. 15 (2013) 3273–3278.
[14] F. Dong, L.Hui L.Xiujuan, X. Weilin, J. Ming, L. Wenbin, F. Xin, Sci Rep, 7 (2017) 1–9.
[15] T.M. do Prado, F.L. Silva, G. Grosseli, P.S. Fadini, O. Fatibello-Filho, F.C. Moraes, Mater., 13 (2020) 1–12.
[16] B.O. Orimolade, O.A. Arotiba, Electrocatalysis 10 (2019) 429–435.
[17] B.O. Orimolade, O.A. Arotiba, J. Electroanal Chem. 878 (2020) 1–18.
[18] L. Xia, J. Bai, J. Li, Q. Zeng, L. Li, B. Zhou, Appl. Catal. B 204 (2017) 127–133.
[19] W.D. Chemelewski, H.C. Lee, J.F. Lin, A.J. Bard, C.B. Mullins, J. Am. Chem. Soc. 136 (2014) 2843–2850.
[20] C.H.A. Tsang, K. Li, Y.X. Zeng, W. Zhao, T. Zhang, Y.J. Zhan, R.J. Xie, D.Y. C. Leung, H.B. Huang, Environ. Int. 125 (2019) 200–228.
[21] L.H. Mascaro, A. Pockett, J.M. Mitchels, L.M. Peter, P.J. Cameron, V. Celorrio, D. J. Fermin, J.S. Sagu, K.G.U. Wijayantha, G. Kociok-Köhn, F. Marken, J. Solid State Electrochem. 19 (2015) 31–35.
[22] R.L. Frost, D.A. Henry, M.L. Weier, W. Martens, J. Raman Spectrosc. 37 (2006) 722–732.
[23] M.R. da Silva, L.H. Dall'Antonia, L.V.A. Scalvi, D.I. dos Santos, L.O. Ruggiero, A. Urbano, J. Solid State Electrochem. 16 (2012) 3267–3274.
[24] M. Wang, C. Niu, J. Liu, Q. Wang, C. Yang, H. Zheng, J. Alloys Compd. 648 (2015) 1109–1115.
[25] T.-F. Yeh, J. Cihlář, C.-Y. Chang, C. Cheng, H. Teng, Materials Today, 16 (2013) 78–84.
[26] W. Zhang, H. Bai, Y. Zhang, Y. Sun, S. Lin, J. Liu, Q. Yang, X.-M. Song, Mater. Chem. Phys. 147 (2014) 1140–1145.
[27] F. Zeng, Z. Sun, X. Sang, D. Diamond, K.T. Lau, X. Liu, D.S. Su, Chem. Sus. Chem. 4 (2011) 1587–1591.
[28] A.C. Johnson, J.P. Sumpter, Environ. Sci. Technol. 35 (2001) 4697–4703.
[29] G. Archana, R. Dhodapkar, A. Kumar, Environ. Monit. Assess. 189 (2017) 446.

[30] K. Nodler, M. Tsakiri, M. Aloupi, G. Gatidou, A.S. Stasinakis, T. Licha, Environ. Pollut. 211 (2016) 282–290.
[31] P. Paiga, C. Delerue-Matos, Mar. Pollut. Bull. 120 (2017) 355–363.
[32] J.P.S. Sidhu, W. Ahmed, W. Gernjak, R. Aryal, D. McCarthy, A. Palmer, P. Kolotelo, S. Toze, Sci. Total Environ. 463 (2013) 488–496.
[33] I.J. Buerge, T. Poiger, M.D. Müller, H.-R. Buser, Environmental Science & Technology, 37 (2003) 691–700.
[34] M.A. de Araujo, D. Coelho, L.H. Mascaro, E.C. Pereira, J. Solid State Electrochem. 22 (2018) 1539–1548.
[35] C. Ravidhas, A.J. Josephine, P. Sudhagar, A. Devadoss, C. Terashima, K. Nakata, A. Fujishima, A.M.E. Raj, C. Sanjeeviraja, Mater. Sci. Semicond. Process. 30 (2015) 343–351.
[36] T.M. do Prado, F.H. Cincotto, O. Fatibello, F. de Moraes, Electroanalysis 30 (2018) 2704–2711.
[37] F.C. Moraes, R.G. Freitas, R. Pereira, L.F. Gorup, A. Cuesta, E.C. Pereira, Carbon 91 (2015) 11–19.
[38] M. Nowak, B. Kauch, P. Szperlich, Rev. Sci. Instrum. 80 (2009).
[39] M. Lamers, W.J. Li, M. Favaro, D.E. Starr, D. Friedrich, S. Lardhi, L. Cavallo, M. Harb, R. van de Krol, L.H. Wong, F.F. Abdi, Chem. Mat. 30 (2018) 8630–8638.
[40] M.S. Fuhrer, C.N. Lau, A.H. MacDonald, MRS Bull. 35 (2011) 289–295.
[41] G. Navarra, M. Moschetti, V. Guarrasi, M. Mangione, V. Militello, M. Leone, Journal of Chemistry 2017 (2017).
[42] C. Indermuhle, M.J. Martín de Vidales, C. Sáez, J. Robles, P. Cañizares, J.F. García-Reyes, A. Molina-Díaz, C. Comninellis, M.A. Rodrigo, Chemosphere 93 (2013) 1720–1725.
[43] I. Dalmázio, L.S. Santos, R.P. Lopes, M.N. Eberlin, R. Augusti, Environ. Sci. Technol. 39 (2005) 5982–5988.
[44] J.P. Telo, A.J.S.C. Vieira, Journal of the Chemical Society, Perkin Transactions 2 (1997) 1755–1758.